Bauxitization and REE Redistribution in Weathered I-type Granite Profile of Gunung Kijang, Bintan Island

Ronaldo Irzon[1,*], Eko Yulianto[2], Hidayat[1] & Firdaus Djabar[3]

[1]Center for Geological Survey, Geological Agency of Indonesia, Jl. Diponegoro 57, Bandung, 40122, Indonesia
[2]Research Center for Geological Hazards, National Research and Innovation Agency of Indonesia, Jl. Sangkuriang Bandung 40135, Indonesia
[3]Research Center for Mining Technology, National Research and Innovation Agency of Indonesia, Jl. Sangkuriang, Bandung, 40135, Indonesia
*E-mail: ronaldoirzon18@gmail.com

Abstract. Weathering is often linked to economic mineral enrichment, including nickel, bauxite, and rare earth elements (REE). The exposed granitic rocks on Bintan Island, Riau Islands Province, belong to the Southeastern Asian Eastern Granite Province. This study examines the bauxitization process and REE distribution across weathered granite horizons in the Gunung Kijang area. Major oxides were analyzed using X-ray fluorescence, while trace and rare earth elements were determined by inductively coupled plasma–mass spectrometry. The trace element composition and metaluminous nature of the parent granite confirm its I-type classification. Kaolinization and bauxitization were observed in the weathered layers, with Al_2O_3 and Fe_2O_3T contents ranging from 25.21–46.50% and 6.99–8.76%, respectively. Total REE content in the weathered horizons (up to 76 ppm) is lower than in the parent rock (214 ppm). Nevertheless, the soft, near-surface materials offer potential for future REE utilization. Clay minerals are the main REE hosts, while the enrichment from the C-horizon upward is influenced by higher organic matter near the surface. Similar Eu and Ce anomaly patterns indicate minimal feldspar in the original granite or limited feldspar breakdown during weathering.

Keywords: *bauxitization; geochemistry; Gunung Kijang; I-type granite; weathering.*

1 Introduction

Weathering is defined as the process of rocks and minerals breaking down or dissolving on Earth's surface. weathering. The activity is enhanced by various agents, namely water circulation, temperature change, plants, animals, and human activities [1-3]. Previously ignored, weathering tends to be worth noticing, because it is correlated to economically valuable materials. Laterite nickel, which appears after the weathering of Ni-rich basic-ultrabasic rocks, is attractive because it is relatively easy to mine and process [4,5]. Bauxite deposits are formed because of intense lateritic weathering of aluminosilicate parent rock

Received March 31st, 2025, Revised August 4th, 2025, Accepted for publication September 19th, 2025
 ISSN: 2337-5760, DOI: 10.5614/j.math.fund.sci.2025.57.1.3

[6,7]. After an investigation in southeastern Asia, [8] proposed ion adsorption-type rare earth elements deposits in which REE are relatively enriched in the specific weathered layer. Weathering is highly effective in tropical climates because of the humidity and the amount of sunlight duration.

The rare earth elements (REE) group consists of the elements in the lanthanide group of the Periodic Table. Further, previous writers have also categorized scandium (Sc) and yttrium (Y) as REE, due to their similar chemical and physical properties [9-12]. The trivalent charge and similar ionic radii of the members of this group make them commonly found together in Earth's crust. The unique behavior of REE has opened a deeper understanding of the geochemical process in Earth's evolution. This group shows the signature of their provenance in various sedimentary sequences [13-15]. The REE spider diagram is important for investigating magma differentiation [16-18]. Chemical analyses of REE have been addressed to help understanding paleo-environments and mass transfer during weathering [4,19,20].

Potential sources of REE cover a wide range of geologic conditions. In igneous rock, large REE deposits are found in carbonatites and alkaline rocks. The first type contains high concentrations of Na- and K-bearing minerals of within-plate tectonic settings, while the second type comprises ≥50% carbonate minerals in deep-seated structural zones of regional extension [18,21]. REE-rich monazite might be deposited in fluvial and coastal environments that originated from metamorphic and (or) igneous bedrock erosions, as reported in the Drava River (Slovenia) and Greece [22,23]. As discussed above, [8] identified REE enrichment in weathered granite, called an ion-adsorption type deposit. This study encouraged more investigation into REE on weathered granite profiles, e.g., in Goias (Brazil), Sulawesi (Indonesia), Kuantan (Malaysia), and South China [24-27].

Granitic rocks in Southeast Asia are categorized into three major provinces, namely, the Eastern, the Main Range, and the Western Province [28-30]. Granite in Bintan is part of the Eastern Province based on its tectonic and geochemistry characters [16]. Bintan Island is an Indonesian island situated south of the Malay peninsula in the Southeast Asian Eastern Granite Province area. I-type granite containing medium abundance of REE occurs on the island [16]. The tropical climate enhances the weathering process on the island and strongly redistributes the rock's chemical composition. The present study evaluated the bauxitization process and REE redistribution of various horizons in a weathered granite profile in the Gunung Kijang region on Bintan Island.

1.1 Geology of Bintan Island

Bintan Island is part of Riau Islands Province and is built of igneous, sedimentary, and metamorphic rocks. The low-grade metamorphic Berakit Formation, formed in the Perm-Carbon age, is the oldest rock unit on the island. The bedrock consists of phyllite, slate, and schist, and is outcropped at the southwest tip of the island. Granitic rocks intruded the Berakit Formation in the Triassic Age. Reference [28] argues that two facies of intrusions can be identified in Bintan, namely, East Bintan granite and Lagoi granite. The geochemistry characteristics of the pinkish Lagoi Granite is explained in [16], but no details on geochemistry data of the East Bintan Granite are available.

Andesite of the Miocene age occurs as small bodies in the central region of Bintan. The Guongon Formation is the largest rock unit on the island and was deposited in the Plio-Pleistocene. The sediment is 200 m thick and consists of tuffaceous sand, tuffaceous lithic, and siltstone. The Holocene Alluvium can only be spotted in a small area near Teluk Bintan. The geological structures in Bintan are in the form of folds, joints, and faults. Some of the structures appear as geomorphological lineaments. The geology of Bintan Island is depicted in Fig. 1.

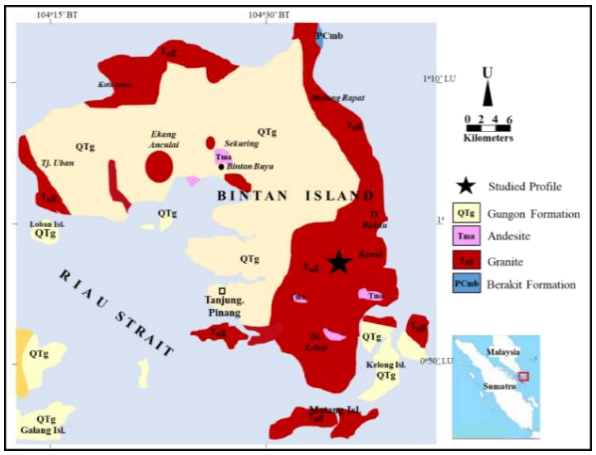

Figure 1 Rock units on Bintan Island, which majorly comprises of the Gungon Formation and granite.

2 Methodology

2.1 Profile Description

The profile studied in this research is situated in Kawal, Gunung Kijang District on Bintan Island. The parent rock of the weathered profile is not directly

outcropped at this station. A light-grey, coarse-grained, and fresh granitic rock was found at about 20 m from the profile. Because the geological map of Bintan places this location in the granite domain, we considered the hard rock as the indirect source rock of the studied profile. The granitic rock is composed of quartz and K-feldspar with a small amount of biotite.

Five horizons in the profile, namely saprolite, lower laterite, middle laterite, upper laterite, and soil, can be distinguished based on color, grain size, and hardness. BINR 16-A was attained from the lowest layer (A-horizon), with a thickness of 1.5 m. This horizon was categorized as saprolite, because coarse quartz grains can be detected easily in this horizon (Figure 2). The high amount of quartz in this layer strengthens the above hypothesis that granite is the parent rock of the studied profile. Quartz grains are still visible in the B-horizon (lower laterite, sample BINR 16-B), but decrease in number and are relatively smaller than in the A-horizon. The lower laterite has a thickness of 1 m and is more reddish than the saprolite. The C-horizon (middle laterite, sample BINR 16-C) is the darkest layer of the studied profile. No more quartz grains are visible in this 1.2 m thick horizon. The upper laterite (D-horizon, sample BINR 16-D) has an average thickness of 0.9 m and shows a brighter red color than horizon C. Plant roots were found in the brownish-red and 0.7 m thick E-horizon (soil layer, sample BINR 16-E).

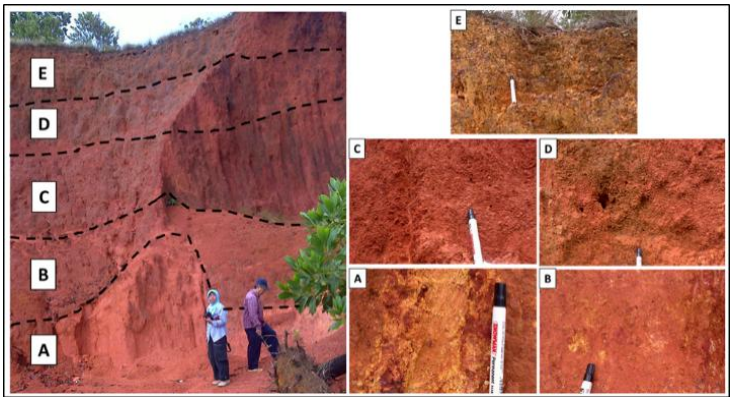

Figure 2 Field conditions of the studied profile. Five weathered horizons were identified in the profile.

2.2 Analytical Procedure

The collected granite and sample of weathered horizons were sent for analysis to the Laboratory of the Center for Geological Survey in Bandung. X-ray fluorescence (XRF) and inductively coupled plasma–mass spectrometry (ICP-

MS) were the two analytical methods used in this work. The hard rock was washed and cleaned of impurities before letting it dry outdoor for one day. On the other hand, samples from the weathering horizon were directly spread thinly on a plastic sheet or tray for air-drying under shade to reduce the rate of possible reactions [4,31]. Whole samples were then crushed with a jaw crusher and were grounded using a ball mill to a gain particle size of 200 mesh. Pressed pellets were analyzed with the Advant XP X-ray fluorescence method (XRF) for their major oxides composition (SiO_2, TiO_2, Al_2O_3, Fe_2O_{3T}, MnO, CaO, MgO, Na_2O, K_2O, and P_2O_5).

A quadrupole iCAP-Q Thermo Fisher Scientific ICP-MS was used to measure the trace and rare earth elements contents in the samples. Acid leaching using nitric acid (ultrapure grade), formic acid (ultrapure grade), and perchloric acid (pro-analysis grade) was adopted in the preparation. All lanthanide elements, except for Pr, as well as six other trace elements (V, Rb, Y, Ba, Th, and U) were analyzed. The counts per second (CPSs) of one blank and six levels of calibration solution (0.1, 1, 5, 10, 25, and 50) were measured to produce the calibration curves of the analyzed elements. The element CPSs of the samples were transformed to concentration by a computer device, adopting the associated calibration curve. This study also prepared and measured two certified reference materials (AGV-2 and GBW 7112) to certify the quality of the analytical method.

Several values are recommended to measure the degree of weathering, i.e. Loss on Ignition (LOI), Chemical Index of Alteration (CIA), Plagioclase Index of Alteration (PIA), CALMAG, and Mafic Index of Alteration (MIA). The first two methods were applied in this study. The LOI value was attained by comparing the sample mass before and after heating at 1,000 °C for an hour [31]. The CIA was calculated using Equation (1) below:

$$CIA = \frac{Al_2O_3}{(Al_2O_3 + CaO^* + Na_2O + K_2O)} x100 \quad (1)$$

Al2O3, Na2O, and K2O are the molecular components in the sample, while CaO is the count of CaO incorporated in the silicate fraction of the rock. CIA variation denotes the feldspar and clay minerals composition in a rock.

3 Results and Discussion

3.1 Analytical Results

The major oxides with trace and REE compositions found in the studied samples are given in Table 1. The parent hard rock mainly consists of SiO_2 (69.47%), Al_2O_3 (13.38%), and Fe_2O_{3T} (4.44%). It is fresh, with a very low LOI of <<2%

(0.76%). In comparison to the parent rock, a drastic decrease in SiO_2 composition is indicated in all layers of the weathered profile, with the lowest detected in the E-horizon (24.58%). On the other hand, sharp increases in Al_2O_3 and Fe_2O_{3T} abundance are seen in the weathered horizons. Peak Al_2O_3 value is detected in the top layer (46.50%), while the C-horizon has the highest Fe_2O_{3T} abundance (8.76%). The high composition of volatile substances in any weathered sample is indicated by a high LOI, which ranged from 8.72% to 19.06%. These numbers are more than 25-fold higher than in the parent rock.

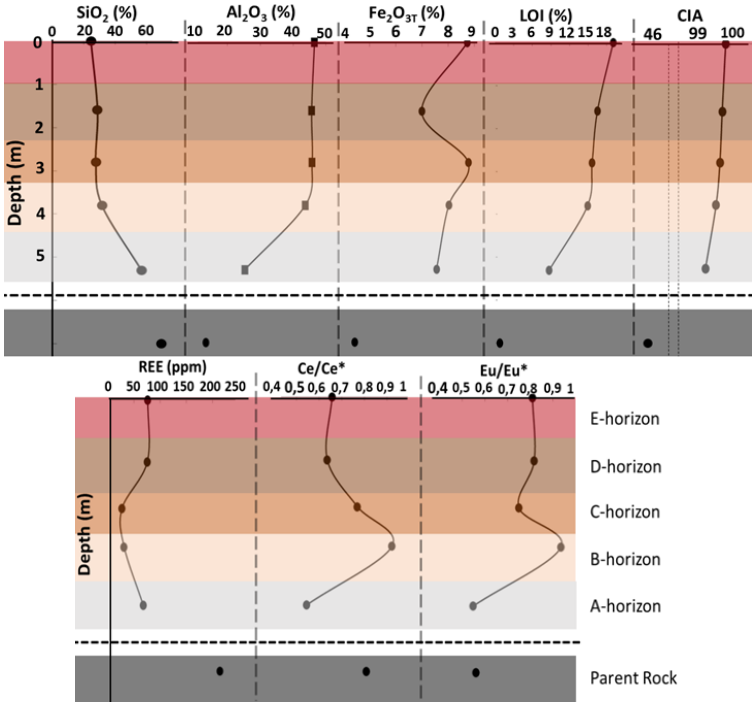

Figure 3 Trends of some selected oxides and elements during weathering. A decrease in SiO_2 abundance during weathering was identified, while Al_2O_3, Fe_2O_{3T}, LOI, and CIA tend to rise.

High CIA values in the weathered horizon indicate the removal of labile cations relative to stable residual constituents during weathering, while low CIA numbers imply low chemical alteration [33,34]. Table 2 shows that the CIA value of the fresh rock (46.33) is much lower than that of any of the weathered samples (98.81-99.79). The CIAs of the weathered horizons show a clear increase from saprolite to soil. The identical increase from the bottom to the top horizon was also amplified by the LOI values, as another parameter in the weathering

evaluation. CIA of fresh, lowly weathered, and moderate to significantly weathered rocks was assumed <50, 50-70, and >70, respectively [35,36]. It was confirmed that the parent rock in this study is relatively fresh, while all samples from the other horizons were significantly weathered. The composition change from fresh granite to all five weathered horizons is shown in Figure 3.

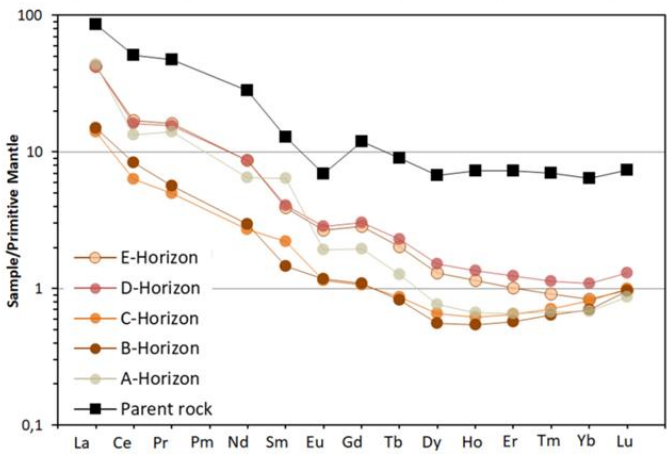

Figure 4 REE normalized pattern against the chondrite value of the studied samples.

The studied parent rock shows a medium value of total REE at 214 ppm. The REE concentration in the weathered layers was lower than in the parent rock, at 27 ppm to 76 ppm. The REE contents in all samples was normalized using the chondrite value of [37] to draw a spider diagram and to determine the Ce/Ce* and Eu/Eu*. REE tendencies are useful to investigate silicate rock formation and element behavior in weathered layers during weathering [4,19,26]. The REE spider diagram of the parent hard rock and all five weathered layers is shown in Figure 4. Light-REE (LREE) shows a sharp negative slope from La to Sm, while the slope of Heavy-REE (HREE) is relatively flat. Ce/Ce* and Eu/Eu* values were counted based on Equation (2) and Equation (3), respectively.

$$\frac{Ce}{Ce} = \sqrt{\frac{Ce_N^2}{La_N^2 x Pr_N^2}} \tag{2}$$

$$\frac{Eu}{Eu} = \sqrt{\frac{Eu_N^2}{Sm_N^2 x Gd_N^2}} \tag{3}$$

REEN is the normalized result of a specific REE composition in any sample to the chondrite value. Fresh rock and weathered horizons denote a negative Ce anomaly and a negative Eu anomaly (Figure 4) in the range of 0.55 (Horizon A) to 0.92 (Horizon B) and 0.55 (Horizon C) to 0.94 (Horizon B), respectively.

Tabel 1 Compositions of parent rock and weathered horizons of the studied profile in Kawal, Bintan Island.

	Parent Rock	A-horizon	B-horizon	C-horizon	D-horizon	E-horizon
Major oxides (%)						
SiO_2	69.47	56.76	31.59	27.69	28.79	24.58
TiO_2	0.31	0.47	1.02	1.11	0.90	0.88
Al_2O_3	13.38	25.21	43.69	45.77	45.63	46.50
Fe_2O_{3T}	4.44	7.55	8.02	8.76	6.99	8.72
MnO	0.08	0.02	0.02	0.01	0.01	0.01
CaO	3.21	0.01	0.01	0.01	0.01	0.01
MgO	1.02	0.09	0.02	0.03	0.02	0.03
Na_2O	3.11	0.01	0.01	0.01	0.01	0.01
K_2O	4.18	0.25	0.24	0.18	0.13	0.06
P_2O_5	0.19	0.04	0.06	0.07	0.11	0.04
LOI	0.76	8.72	14.91	15.66	16.51	19.06
Trace and rare earth elements (ppm)						
V	9.56	19.11	23.01	23.40	23.31	25.35
Ga	5.94	11.88	17.32	18.21	18.17	16.46
Rb	10.14	20.27	23.04	15.38	10.41	4.77
Sr	5.34	10.68	6.27	7.11	17.62	15.51
Y	0.81	1.63	1.45	1.67	3.38	2.76
Nb	2.55	5.09	27.85	24.06	20.77	34.75
Cs	0.46	0.91	0.67	0.64	0.56	0.48
Ba	16.82	33.65	22.67	16.92	25.83	27.19
La	14.18	28.36	9.73	9.09	27.43	27.32
Ce	11.20	22.41	14.02	10.62	27.06	28.39
Pr	1.79	3.57	1.43	1.26	3.97	4.11
Nd	4.08	8.16	3.68	3.38	10.85	10.89
Sm	1.30	2.60	0.59	0.90	1.65	1.58
Eu	0.15	0.30	0.18	0.18	0.44	0.41
Gd	0.53	1.05	0.59	0.58	1.64	1.54
Tb	0.06	0.13	0.08	0.09	0.23	0.20
Dy	0.26	0.52	0.37	0.44	1.02	0.87
Ho	0.05	0.10	0.08	0.09	0.20	0.17
Er	0.14	0.29	0.25	0.28	0.54	0.44
Tm	0.02	0.05	0.04	0.05	0.08	0.06
Yb	0.15	0.30	0.31	0.36	0.48	0.37
Lu	0.03	0.06	0.07	0.07	0.09	0.07
Tl	0.05	0.09	0.09	0.57	0.05	0.03
Th	27.23	54.46	51.64	58.95	61.12	47.45
U	2.62	5.23	17.01	19.40	13.63	8.01

3.2 Parent Rock Classification

Alphabetically, granitic rocks are classified into I-, S-, A-, and M-types. I-type intrusion is collision-associated, while S-type one is initiated by subduction. An anoroganic environment inducts A-type granite, while the M-type is generally sourced from the mantle. Previous studies concluded that the granite in Bintan Island is I-type, because it was crystallized after the Sibumasu and East Malaya collision [28,32].

The Y, Nb, Ce, and Zn compositions of the selected rock are much lower than 10 ppm, 20 ppm, 85 ppm, and 100 ppm, respectively (Table 2), excluding it from A-type granite [16]. A/CNK is widely used in rock evaluation and its value can be calculated using Equation 4 below:

$$A/CNK = \frac{Al_2O_3}{CaO + Na_2O + K_2O} \quad (4)$$

Rocks with A/CNK values >1 are called peraluminous, while ones with A/CNK values <1 are called metaluminous. Moreover, A/CNK differentiates I-type from S-type intrusion, where A/CNK<1.1 is typical for I-type granite, while >1.1 is categorized into the S-type. The studied parent hard rock is clearly I-type metaluminous granite with A/CNK 0.86. This result confirms previous studies about the alphabetic granite type in Bintan.

3.3 Bauxitization and REE Mobilization

The accumulation of Al_2O_3 and Fe_2O_{3T} with SiO_2 depletion is affected by the rise of weathering intensity. This assumption is the basis of the lateritization triangular diagram. Moreover, these three oxides' composition was utilized to determine the formation of kaolin, bauxite, and ferrite in the weathered horizons [38]. It was seen that the saprolite (A-horizon) experienced kaolinization, while the other weathered layers were lateritized moderately (Figure 5a). The sample from Horizon A falls within the bauxitic-kaolinite field, while the others are on the border between bauxite and kaolinitic-bauxite (Figure 5b). Bauxite formation in this profile is correlated with the fact that Bintan is a bauxite-producing island, especially in Gunung Kijang District.

Weathering surely redistributes chemical components in the parent rock and its weathered horizons. The REE in the weathered layers is sourced from REE-bearing bedrock. Several processes influence REE redistribution during weathering, e.g., its reaction with groundwater during circulation, the partition into solid phase, and REE sorption onto the surface of minerals (Mn-Fe hydroxides, phosphate minerals, and clay minerals). All members of REE are present in a 3+ redox state, except for Ce and Eu, which can also exist in Ce^{4+}

and Eu^{2+}. Ce^{3+} can be oxidized to Ce^{4+} after reacting with atmospheric oxygen in alkaline conditions. Eu^{2+} is formed after feldspar breakdown and is relatively mobile, while Eu^{3+} is immobile. However, Eu^{2+} can be carried away by groundwater in a dissolved state.

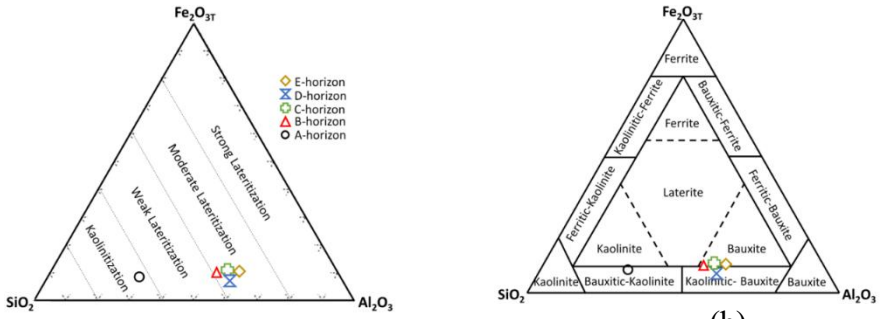

Figure 5 SiO_2-Fe_2O_{3T}-Al_2O_3 triangular diagram of samples from weathered horizons in Gunung Kijang: a) Horizon A is kaolinitized, while the other horizons are lateritized moderately; b) Horizon A is classified as bauxitic-kaolinite, while the others are on the border between bauxite and kaolinitic-bauxite.

The increase of the REE content with the addition of Al_2O_3 components in the studied profiles imply that clay minerals are the most common hosts of REE [39,40]. The lowest REE content in the A-horizon is influenced by its lowest clay mineral composition (Al_2O_3). Horizon A contains almost the same amount of REE as the Horizon B, but a significant REE increase was detected in Horizon C. The Ce anomaly is more positive in the Horizon B than in Horizon A, but it drops in Horizon C. These facts illustrate the oxidized Ce remaining in Horizon B, while the other REE was transported upward to Horizon C. REE adsorption in Horizon C is enhanced by its high clay mineral composition according to the increase of the Al_2O_3 content. The elevated REE composition from Horizon C continuously to Horizon D and E may have been helped by the high organic matter content at the top of the profile [41]. The Eu anomaly shows a similar pattern as the Ce anomaly, implying that the host rock contains a minimum amount of feldspar or no significant feldspar breakdown happened during bauxitization in this profile.

4 Conclusion

A granitic parent rock and its weathered samples from five horizons from Gunung Kijang were studied and measured for their chemical composition. The parent rock shows I-type granite characteristics with A/CNK <1.1 and low Y, Nb, Ce, and Zn compositions. The LOI and CIA values indicate that the parent granite is

relatively fresh, while the other samples were weathered. Significant Al_2O_3 enrichment in the weathered layers emphasizes the bauxitization process on the profile, with a maximum Al_2O_3 of 46.50%. Although the REE content in the weathered horizons was lower than in the fresh rock, its softness and placement near the surface make it worthwhile for future mining. The REE in the weathered horizons was mainly contained in clay minerals. Organic matter at the top of the profile has helped REE movement from horizon C upward. The granite parent rock should contain minimum feldspar or only a small feldspar breakdown happened during weathering according to similar Eu/Eu* and Ce/Ce* patterns from the weathered horizons.

5 Acknowledgements

The writers would like to thank the head of the Center for Geological Survey of Indonesia for publication permission. Mr Sigit Maryanto and Mr Joko Subandrio are acknowledged for their review of Bintan geology. Mrs Irfanny Agustiany helped with excellent laboratory assistance.

References

[1] Tating, F., Hack, R. & Jetten, V., *Weathering Effects on Discontinuity Properties in Sandstone in a Tropical Environment: Case Study at Kota Kinabalu, Sabah Malaysia*, Bulletin of Engineering Geology and the Environment, **74**, pp. 427-441, 2015.

[2] McAllister, D., Warke, P. & McCabe, S., *Stone Temperature and Moisture Variability Under Temperate Environmental Conditions: Implications for Sandstone Weathering*. Geomorphology, **280**, pp. 137-152, 2017.

[3] Korkanç, M., İnce, İ., Hatır, M.E. & Tosunlar, M.B., *Atmospheric and Anthropogenic Deterioration of the İvriz Rock Monument: Ereğli-konya, Central Anatolia, Turkey*. Bulletin of Engineering Geology and the Environment, **80**, pp. 3053-3063, 2021.

[4] Irzon, R. & Abdullah, B., *Element Mobilization During Weathering Process of Ultramafic Complex in North Konawe Regency, Southeast Sulawesi based on a Profile from Asera*, Indonesian Journal on Geoscience, **5**(3), pp. 277-290, 2018.

[5] Tupaz, C.A.J., Watanabe, Y., Sanematsu, K. & Echigo, T., *Spectral and Chemical Studies of Iron and Manganese Oxyhydroxides in Laterite Developed on Ultramafic Rocks,* Resource Geology, **71**(4), pp. 377-391, 2021.

[6] Kusin, F.M., Azani, N.N.M., Hasan, S.N.M.S. & Sulong, N.A., *Distribution of Heavy Metals and Metalloid in Surface Sediments of Heavily-mined Area for Bauxite Ore in Pengerang, Malaysia and Associated Risk Assessment*, Catena, **165**, pp. 454-464, 2018.

[7] Boeva, N., Bortnikov, N., Slukin, A., Shipilova, E., Makarova, M. & Melnikov, P., *Biofilms and Biominerals in the Lateritic Weathering Crust as Exemplified by the Central Bauxite Deposit (Siberian Platform, Russia)*, Minerals, **11**(11), 1184, 2021

[8] Sanematsu, K., Kon, Y., Imai, A., Watanabe, K. & Watanabe, Y., *Geochemical and Mineralogical Characteristics of Ion-adsorption Type REE Mineralization in Phuket, Thailand*, Mineralium Deposita, **48**, pp. 437-451, 2013.

[9] Voncken, J.H.L., *The Rare Earth Elements: An Introduction*, Cham, Switzerland: Springer International Publishing, 2016.

[10] Mosai, A.K. & Tutu, H., *Simultaneous Sorption of Rare Earth Elements (Including Scandium and Yttrium) from Aqueous Solutions using Zeolite Clinoptilolite: A Column and Speciation Study*, Minerals engineering, **161**, 106740, 2021.

[11] Yuksekdag, A., Kose-Mutlu, B., Kaya, B., Kumral, M., Wiesner, M.R. & Koyuncu, I., *Comprehensive Characterization of Secondary Sources Originating from Turkey in Terms of Rare Earth Elements and Scandium*, Science of The Total Environment, **777**, 146033, 2021.

[12] Irzon, R., Kurnia, Haryanto, A.D., Maryanto, S. & Hernawan, U., *Distinct Depositional Environments of Two Internal Reference Materials with Marine Sediment Matrix from Nearby Bangka Island*, Bulletin of the Geological Society of Malaysia, **73**, pp. 181-189, 2022.

[13] Ferdous, N. & Farazi, A.H., *Geochemistry of Tertiary Sandstones from Southwest Sarawak, Malaysia: Implications for Provenance and Tectonic Setting*, Acta Geochimica, **35**, pp. 294-308, 2016.

[14] Irzon, R., Syafri, I., Agustiany, I., Prabowo, A. & Sendjaja, P., *Petrology and Geochemistry of the Volcanic Arc Tarusan Pluton in Comparison to Lolo Pluton, West Sumatra*, Jurnal Geologi dan Sumberdaya Mineral, **20**(4), pp. 199-210, 2019.

[15] Barber, A.J., Crow, M.J. & Milsom, J. (Eds.), *Sumatra: Geology, Resources and Tectonic Evolution,* Geological Society of London, 2005.

[16] Ahnaf, J.S., Patonah, A. & Permana, H., *Petrogenesis of Volcanic Arc Granites from Bayah Complex, Banten, Indonesia*, Journal of Geoscience, Engineering, Environment, and Technology, **4**(2), pp. 104-115, 2019.

[17] Waight, T., Fyhn, M.B., Thomsen, T.B., Van Tri, T., Nielsen, L.H., Abatzis, I. & Frei, D., *Permian to Cretaceous Granites and Felsic Volcanics from SW Vietnam and S Cambodia: Implications for Tectonic Development of Indochina*, Journal of Asian Earth Sciences, **219**, 104902, 2021.

[18] Zoheir, B. & Diab, A., *Origin of the Volcanic-arc Signature in Late-Orogenic Granitoids from the Arabian–Nubian Shield, In the Geology of the Arabian-Nubian Shield,* Springer, Cham., (pp. 439-450), 2021.

[19] Amin, T.C., Sidarto, Santosa, S. & Gunawan, W., *Peta Geologi Lembar Kotaagung, Sumatra, Skala 1:125.000,* Pusat Penelitian dan Pengembangan Geologi, Bandung, 1993.
[20] Acocella, V., Bellier, O., Sandri, L., Sébrier, M. & Pramumijoyo, S., *Weak Tectono-magmatic Relationships along an Obliquely Convergent Plate Boundary: Sumatra, Indonesia*, Frontiers in Earth Science, **6**, 3, 2018.
[21] Irzon, R., *Comagmatic Andesite and Dacite in Mount Ijo, Kulonprogo: A Geochemistry Perspective*, Jurnal Geologi dan Sumberdaya Mineral, **19**(4), pp. 221-231, 2018.
[22] Irzon, R., Maryanto, S., Syafri, I., Kurnia, Jazuli, H.H. & Hartanto, P., *Wackestones and Grainstones Geochemistry from Baturaja Formation, South Sumatra Province, Indonesia: Origin and Depositional Environment*, Sains Malaysiana, **51**(4), pp. 1005-1015, 2022.
[23] Maulana, A., Watanabe, K. & Yonezu, K., *Petrology and Geochemistry of Granitoid from South Sulawesi, Indonesia: Implication for Rare Earth Element (REE) Occurrences*, International Journal of Engineering and Science Applications, **3**(1), pp. 79-86, 2016.
[24] Nualkhao, P., Takahashi, R., Imai, A. & Charusiri, P., *Petrochemistry of Granitoids Along the Loei Fold Belt, Northeastern Thailand*, Resource Geology, **68**(4), pp. 395-424, 2018.
[25] Abdel Gawad, A.E., *Mineral Chemistry (U, Th, Zr, REE) in Accessory Minerals from Wadi Rod Elsayalla Granitoids, South Eastern Desert, Egypt*, Arabian Journal of Geosciences, **14**(19), pp. 1-17, 2021.
[26] Cox, K.G., Bell, J.D. & Pankhurst, R.J., *Compositional Variation in magmas. In the Interpretation of Igneous Rocks,* Springer Dordrecht, (pp. 12-41), 1979.
[27] Irvine, T.N. & Baragar, W.R.A., *A Guide to the Chemical Classification of the Common Volcanic Rocks*, Canadian Journal of Earth Sciences, **8**(5), pp. 523-548, 1971.
[28] Chappell, B.W., *Source Rocks of I-and S-type Granites in the Lachlan Fold Belt, Southeastern Australia*, Philosophical Transactions of the Royal Society of London. Series A, Mathematical and Physical Sciences, **310**(1514), pp. 693-707, 1984.
[29] Jafari, A., Fazlnia, A. & Jamei, S., *Geochemistry, Petrology and Geodynamic Setting of the Urumieh Plutonic Complex, Sanandaj–Sirjan Zone, NW Iran: New Implication for Arabian and Central Iranian Plate Collision*, Journal of African Earth Sciences, **139**, pp. 421-439, 2018.
[30] Wu, D., Zheng, K., Wu, C., Chen, H., Gao, D., & Zou, F., *Geochronology and geochemistry of the Bashikaogong S-type Granitic Rocks: A Record of Early Paleozoic Subduction and Collision in North Altun, Northwestern China*, Arabian Journal of Geosciences, **14**, pp. 1-20, 2021.
[31] Yadav, B. S., Ahmad, T., Kaulina, T., Bayanova, T. & Bhutani, R., *Origin of Post-collisional A-type Granites in the Mahakoshal Supracrustal Belt,*

Central Indian Tectonic Zone, India: Zircon U-Pb Ages and Geochemical Evidences, Journal of Asian Earth Sciences, **191**, 104247, 2020.

[32] Regelous, A., Scharfenberg, L., & De Wall, H., *Origin of S-, A-and I-type Granites: Petrogenetic Evidence from Whole Rock Th/U Ratio Variations*, Minerals, **11(**7), 672, 2021.

[33] Setiawan, I., Takahashi, R. & Imai, A., *Petrochemistry of Granitoids in Sibolga and its Surrounding Areas, North Sumatra, Indonesia*, Resource Geology, **67**(3), pp. 254-278, 2017.

[34] Pearce, J.A., Harris, N.B. & Tindle, A.G., *Trace Element Discrimination Diagrams for the Tectonic Interpretation of Granitic Rocks*, Journal of Petrology, **25**(4), pp. 956-983, 1984.

[35] Zhang, H., Hu, P., Cao, L., Tampubolon, A., Liu, A., Cheng, X. & Pan, B., *Geochemical Characteristics and Sr-Nd-Hf Isotope Compositions of Late Triassic Post-collisional A-type Granites in Sarudik, SW Sumatra, Indonesia*, Island Arc, **29**(1), e12357, 2020.

[36] Liu, Y., Lai, J., Xiao, W., Jeffrey, D., Du, R., Li, S. & Yu, X., *Petrogenesis and Mineralization of Two-stage A-type Granites in Jiuyishan, South China: Constraints from Whole-rock Geochemistry, Mineral Composition and Zircon U-Pb-Hf Isotopes*, Acta Geologica Sinica-English Edition, **93**(4), pp. 874-900, 2019.

[37] Frost, B.R., Barnes, C.G., Collins, W.J., Arculus, R.J., Ellis, D.J., & Frost, C.D., *A Geochemical Classification for Granitic Rocks*, Journal of Petrology, **42**(11), pp. 2033-2048, 2001.

[38] Nakamura, N., *Determination of REE, Ba, Fe, Mg, Na and K in carbonaceous and ordinary chondrites*, Geochimica et Cosmochimica Acta, 38(5), pp. 757-775, 1974.

[39] Terekhov, E.N. & Shcherbakova, T.F., *Genesis of Positive Eu Anomalies in Acid Rocks from the Eastern Baltic Shield*, Geochemistry International, **44**(5), pp. 439-455, 2006.

[40] Sun, K., & Chen, B., *Trace Elements and Sr-Nd Isotopes of Scheelite: Implications for the W-Cu-Mo Polymetallic Mineralization of the Shimensi Deposit, South China*, American Mineralogist, **102**(5), pp. 1114-1128, 2017.